Seafloor Pressure Measurements of Nonlinear Internal Waves

J. N. MOUM AND J. D. NASH

College of Oceanic and Atmospheric Sciences, Oregon State University, Corvallis, Oregon

(Manuscript received 7 December 2006, in final form 25 June 2007)

ABSTRACT

Highly resolved pressure measurements on the seafloor over New Jersey's continental shelf reveal the pressure signature of nonlinear internal waves of depression as negative pressure perturbations. The sign of the perturbation is determined by the dominance of the internal hydrostatic pressure (p^0_{Wh}) due to isopycnal displacement over the contributions of external hydrostatic pressure ($\rho_0 g\eta_H$; η_H is surface displacement) and nonhydrostatic pressure (p^0_{nh}), each of opposite sign to p^0_{Wh}. This measurement represents experimental confirmation of the wave-induced pressure signal inferred in a previous study by Moum and Smyth.

1. Introduction

Highly resolved and rapidly sampled measurements of velocity from a fixed position on the seafloor over Oregon's continental shelf led to a prediction of the form, sign, and magnitude of the pressure signature of nonlinear internal waves of elevation (Moum and Smyth 2006). The competing effects of internal hydrostatic pressure (>0 for elevation waves), external hydrostatic pressure, and nonhydrostatic pressure (both <0 for elevation waves) led to a predicted positive seafloor pressure anomaly. It was further inferred that a negative seafloor pressure anomaly would result from the passage of a nonlinear internal wave of depression. As an experimental test of our predictions, we deployed three highly sensitive pressure sensors on the seafloor over the New Jersey shelf in summer 2006 as part of a larger experiment to study the physics of nonlinear internal waves and their effects on acoustic propagation.

The deep ocean acts to low-pass filter the seafloor pressure contribution from deep water surface gravity waves since these pressure signals decay as $e^{k(z-H)}$ (Webb et al. 1991). This permits unambiguous detection of intermittently occurring long-wavelength surface waves in deep water, such as tsunamis (Meinig et al. 2005). However, on continental shelves, the full spectrum of surface gravity waves out to frequencies associated with wind waves can have a significant seafloor pressure signature. This makes detection of intermittently occurring signals such as nonlinear internal waves (Helfrich and Melville 2006) more challenging.

Beyond confirmation of the calculation of pressure from water-column velocity records (Moum and Smyth 2006), these measurements and the accompanying analysis demonstrate the richness of information in highly resolved seafloor pressure measurements. We first define the wave-induced pressure field (section 2). We then describe the pressure measurement (section 3) and how the pressure sensor was deployed, together with complementary measurements (section 4). There follows an examination of the pressure spectrum and its variability on various time scales as well as a comparison of the measured and inferred pressure signals of nonlinear internal waves of depression propagating over the shelf (section 5). A discussion (section 6) and summary (section 7) follow.

2. Definition of the wave pressure at the seafloor

In this section, we summarize the computation of the seafloor pressure signal of a nonlinear internal wave from water-column measurements of density and velocity (Moum and Smyth 2006). Specifically, we consider the seafloor pressure associated with a two-dimensional, nonlinear, nonhydrostatic internal wave traveling in the x direction with phase speed c. This will be

Corresponding author address: J. N. Moum, College of Oceanic and Atmospheric Sciences, Oregon State University, COAS Admin. Bldg. 104, Corvallis, OR 97331-5503.
E-mail: moum@coas.oregonstate.edu

DOI: 10.1175/2007JPO3736.1

compared to the measured seafloor pressure in section 5.

The density is defined as the sum of a background density profile $\rho_o + \rho_b(z)$ and a perturbation associated with the wave, $\rho_w(x, z, t)$:

$$\rho(x, z, t) = \rho_o + \rho_b(z) + \rho_w(x, z, t). \quad (1)$$

The seafloor value of the pressure disturbance resulting from the passage of a nonlinear internal wave is derived by Moum and Smyth (2006) as the sum of internal hydrostatic pressure (due to isopycnal displacement) plus external hydrostatic pressure (due to surface displacement) plus nonhydrostatic pressure (due to vertical fluid accelerations). Vertical integration of the vertical momentum equation leads to

$$p^0 = p^0_{\mathrm{Wh}} + \rho_o g \eta_H + p^0_{\mathrm{nh}}, \quad (2)$$

where the superscript 0 represents the pressure at the seafloor ($z = 0$); $\eta_H(x, t)$ is the wave-induced surface displacement at $z = H$, the height of the undisturbed surface. We consider only the wave's contribution to the internal hydrostatic pressure p^0_{Wh}, defined as

$$p^0_{\mathrm{Wh}} = g \int_0^H \rho_w \, dz'. \quad (3)$$

The nonhydrostatic pressure is

$$p^0_{\mathrm{nh}} = \rho_o \int_0^H \frac{Dw}{Dt} \, dz', \quad (4)$$

where

$$\frac{D}{Dt} \equiv \frac{\partial}{\partial t} + u \frac{\partial}{\partial x} + w \frac{\partial}{\partial z}. \quad (5)$$

The surface displacement is obtained by integrating the horizontal momentum equation along $z = H$. Assuming the surface displacement vanishes at $x = \pm\infty$,

$$\eta_H = -\frac{1}{g} \int_{-\infty}^x \frac{Du_H}{Dt} \, dx', \quad (6)$$

where u_H is the velocity in the direction of wave propagation at $z = H$.

The seafloor pressure is independently estimated by integrating the horizontal momentum equation along $z = 0^+$,

$$p^o_{Du/Dt} = -\rho_o \int_{-\infty}^x \frac{Du_0}{Dt} \, dx', \quad (7)$$

where u_0 is the velocity in the direction of wave propagation at $z = 0^+$. Of course, $u = 0$ at $z = 0$, and we designate this height as $z = 0^+$ although we actually measure u at $z = 3.2$ m, which is the height of the velocity measurement nearest the seafloor. The consequence of this is discussed in section 6.

3. Pressure measurement

A Paroscientific Model 6000–200A pressure transducer was mounted inside a pressure-pod (Ppod), a 15-cm-diameter cylinder that houses sampling electronics, data storage, and batteries. The transducer has a full scale output of 200 psi and a quoted resolution of 1 ppm, equivalent to 2×10^{-4} psi (1.4 Pa, or 0.14-mm surface displacement). Noise tests in our laboratory confirm the noise level of our system to be near to 1 Pa^2 Hz^{-1} over the frequency band 10^{-3}–1 Hz, equivalent to <1 ppm rms. This sensor is similar to that used for deep ocean tsunami detection (Meinig et al. 2005), but is optimized for coastal applications where increased sensitivity is obtained at the expense of reduced dynamic range.

4. Experimental details

As part of the Shallow Water 2006 experiment, a large mooring array was deployed for a 2-month period on the New Jersey shelf to capture oceanographic processes that affect acoustic propagation (Fig. 1). The array was specifically tuned to capture nonlinear internal waves that propagate onto the shelf from the southeast, as these can alter acoustic propagation over a range of frequencies. To measure the structure and evolution of the internal wave field, we deployed four bottom landers, each outfitted with an SBE 37 MicroCat, Sontek acoustic Doppler velocimeter (ADV), and acoustic Doppler current profiler (ADCP) (500-kHz Sontek ADP on SW37 and RD Instruments 300-kHz ADCPs elsewhere). As well, Ppods were added to three landers (SW37, SW38, SW39, as noted in Fig. 1). All of the pressure sensors were sampled at 1 Hz.

During this deployment, we conducted a separate wave-tracking experiment employing shipboard acoustics, radar, and in situ profiling with our turbulence profiler, Chameleon (Moum et al. 1995), from R/V *Oceanus*. Individual wave trains were identified and tracked through the array. Following the tradition of naming tropical storms, significant tracked waves were named. Some of these are identified in the lander-based data discussed here. The profile data also yielded full water-column density profiles that we use here and a 26-h time series near one of our landers (SW37).

5. Results

Before examining the details of the pressure record and isolating the signature of the nonlinear internal

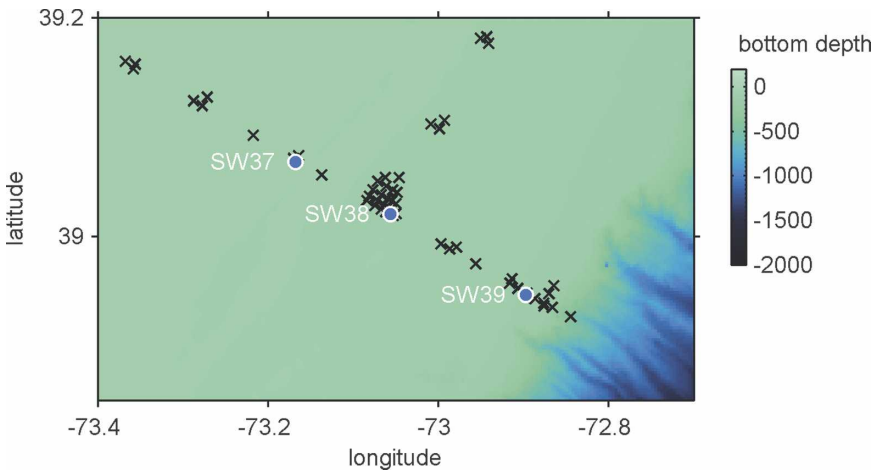

FIG. 1. Mooring locations on the New Jersey shelf deployed July–September 2006 for the Nonlinear Internal Wave/Shallow Water 2006 experiment. Crosses depict moorings not discussed here. High-resolution seafloor pressure measurements were made at SW37 (70-m water depth), SW38 (80-m water depth), and SW39 (110-m water depth). These three locations were oriented along a line in the compass direction 300° from the shelf break. The separation between SW37 and SW38 was 11 km and between SW37 and SW39 it was 27 km.

waves, we first use the dominant low frequency part of the signal to provide background perspective on our observations and the nonlinear internal wave climate at the time of these measurements.

Any pressure record in the ocean is typically dominated by displacements of the free surface at tidal frequencies. The seafloor pressure measured at SW37 (filtered at 1/3000 Hz to emphasize the tides) is shown in Fig. 2a. Our wave-tracking experiment started with the neap tides at the end of July and continued through the following complete spring–neap cycle (Fig. 2a). The largest amplitude waves were observed from ship during 14–25 August, during neap tides. From the ADP vertical velocity record at SW37, nonlinear internal wave events were subjectively selected (79 in all) for the period of the moored observations. These include all of the ship-tracked waves and exhibit various forms, from single solitary-like waves to borelike waves to packets that include dozens of nonlinear internal waves.

While a more complete wave climate analysis that includes all of the moored data and perhaps a more objective means of defining nonlinear internal waves will follow, this analysis indicates a couple of important points. First, more waves were observed at SW37 during the neap tide than either of the two spring tides (wave counts are noted atop Fig. 2a). This is consistent with our wave-tracking observations, at least in the sense that the most easily observed, larger waves were found during the neap. However, we note that, during the tropical storms that dominated the second spring of the moored record (which thankfully did not coincide with our shipboard experiments) either nonlinear internal waves were very rare or simply more difficult to distinguish from other tropical storm-induced motions in the moored record. And, second, waves observed at SW37 were not phase-locked to the barotropic tide; in fact, they were observed at that location at all phases of the tide (Fig. 2b) although there was a greater tendency for waves to be observed at this site at or shortly following low tide.

A raw time series of pressure does not reveal very much about the richness of the physical processes that contribute to the total pressure signal. As an aid in interpretation and to help us determine how to extract the nonlinear internal wave signal, we first examine the power spectrum of pressure, which is dominated by tides and swell. Owing to the ubiquity of surface gravity waves at all frequencies and the severe intermittency of nonlinear internal waves, we will show that the spectral amplitude of internal hydrostatic pressure is small compared to that from the external hydrostatic pressure. The signature of nonlinear internal waves is exposed in a spectrogram, which also helps to define the filtering procedure required to extract the nonlinear internal wave signal. This is then compared to predictions based on density and velocity measurements.

a. The spectrum of pressure on the New Jersey continental shelf in August 2006

Power spectra of 32-day pressure records at each of the three locations clearly show the tidal peaks (semi-

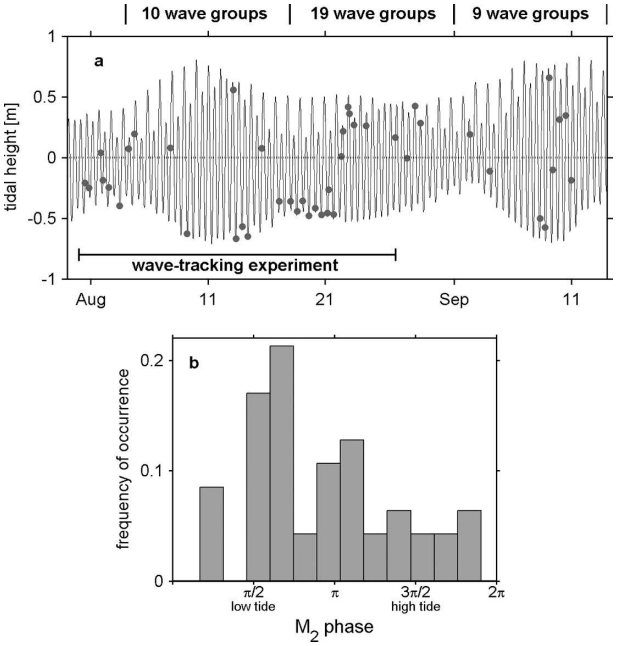

FIG. 2. (a) Measured pressure at SW37, low-pass filtered to emphasize the tidal frequency and plotted as surface displacement (mean removed). The red circles represent nonlinear internal waves identified from the vertical velocity profile record at SW37. To identify waves, the rms value of w was computed for the depth range 12.8–38.8-m height from a 3000-s record by integrating a spectrogram over the frequency bandwidth 0.5–10 mHz. Waves were defined according to a threshold value of 0.015 m s^{-1}. A wave-tracking experiment from R/V *Oceanus* 31 Jul–27 Aug 2006 tracked many of these waves. Above the plot is marked a rough spring–neap–spring cycle as defined by the pressure record. Within each cycle, the number of dots were summed and noted. (b) Frequency of occurrence of nonlinear internal waves relative to tidal phase. The phase was defined so that low tide corresponds to $\pi/2$ and high tide to $3\pi/2$.

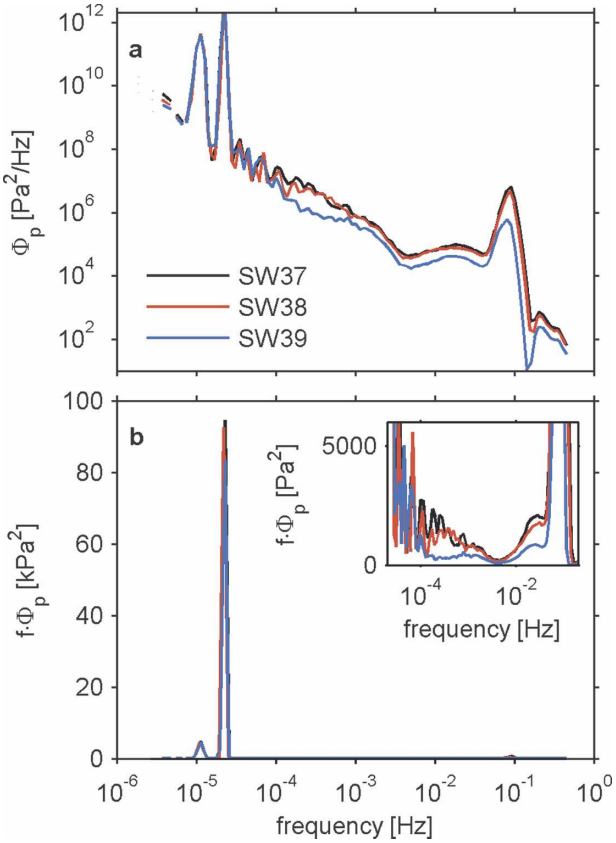

FIG. 3. Line spectra of pressure records obtained at each of the locations shown in Fig. 1. The time period represented here is 30 Jul–31 Aug 2006, prior to two tropical storms observed during the deployments (these are noted in Fig. 5). (a) Amplitude spectra. (b) Variance-preserving spectra; inset is an expanded plot that emphasizes the variance in the frequency range between tides and swell.

diurnal, diurnal) at low frequency and the swell near 0.1 Hz (Fig. 3). These barotropic motions dominate the total variance in the signal (Fig. 3b). Intermediate frequencies are also dominated by surface waves; this is termed the infragravity wave range (Webb et al. 1991). One way to see this is by comparison of spectral amplitudes obtained from measured seafloor pressure at SW37 to the baroclinic hydrostatic pressure determined from a 26-h profiling time series at that location (Fig. 4). Using density profiles obtained at roughly 2-min intervals (yielding a Nyquist frequency of 0.004 Hz), the linear, hydrostatic pressure contribution was computed as $p'(z,t) = p_{\text{surf}} + \int_z^H \rho'(z',t)g\,dz'$ (Kunze et al. 2002; Nash et al. 2005). Here $\rho'(z,t) = \rho(z,t) - \overline{\rho}(z)$ is the wave-induced density perturbation, ($\overline{\rho}(z)$ is the time-mean density), and p_{surf} is determined by satisfying the baroclinicity condition $H^{-1}\int_o^H p'(z,t) = 0$; that is, the depth-averaged perturbation pressure must vanish. For the case of nonlinear, nonhydrostatic waves (Moum and Smyth 2006), p' overestimates the seafloor pressure because hydrostatic and nonhydrostatic terms are of opposite sign in the wave core.

The seafloor pressure due to internal isopycnal displacements is smaller by a factor of at least 10 (and mostly much greater than this) at all resolved frequencies. This in turn suggests that, at least over the continental shelf, the linear internal wave spectrum is not resolved in the measurement, simply due to the overwhelming surface wave signal. Because of the extreme intermittency of the nonlinear internal waves, neither is their pressure signal resolved in the spectrum of equivalent length. However, as is subsequently demonstrated, the nonlinear internal wave pressure signal is clear in spectra from sufficiently short records, or from the time series.

The richness of the signal, at least in the super-mHz range, is revealed in a spectrogram of the record (Fig.

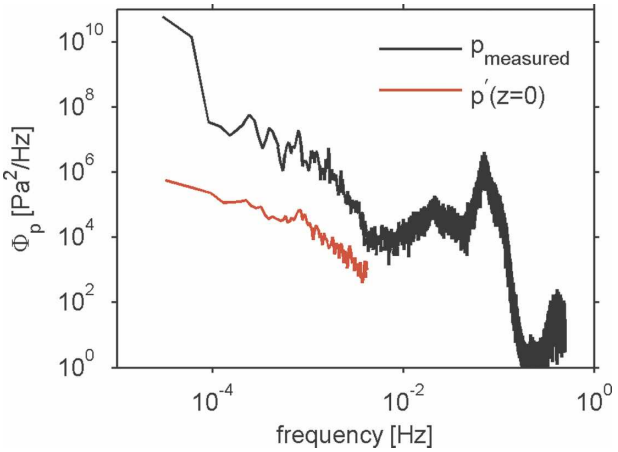

FIG. 4. Comparison of measured seafloor pressure to the internal hydrostatic pressure determined by vertical integration of density measured from a 26-h Chameleon profiling time series.

5d). To aid in interpreting the spectrogram, wind records from R/V *Oceanus* (gray; within the SW06 mooring array) and from a NOAA buoy 350 km east-southeast from SW39 (black) are shown in Fig. 5a. These are reasonably correlated with a small lag and we use the buoy record as representative of the local winds. Significant wave heights from the buoy are also shown. The time series of the full pressure record (Fig. 5c) indicates barotropic tidal oscillations, spring/neap variations of these, and the influence of Atlantic tropical storms.[1] Beyond this, however, this depiction of the time series alone is not particularly revealing.

By computing spectra from relatively short records and combining these into a longer time series (Fig. 5d), we gain an appreciation for both evolving and episodic signals. Five particular bandwidths stand out:

- At frequencies >0.1 Hz, locally generated wind waves contribute to the seafloor pressure signal. These are closely related to measured winds and H_s, the significant wave height obtained from the offshore NOAA 44004 Buoy. The correspondence between the signals at SW37 and the offshore buoy indicates that the wind signal represents a large geographical area.
- The swell is concentrated in the 10–20-s period band. There is a clear modulation of the swell over the record, especially in response to the two named tropical storms, during which the intensity of the short surface gravity waves (mostly swell) serves to obscure the tides in the time series (Fig. 5c). Wave dispersion is evident in the wisplike structures of high amplitudes that increase in frequency over time, signifying the arrival of remotely generated long-period swell in advance of shorter periods. Steeper curves indicate closer storm events.
- Variance in the 20–100-s band (infragravity waves) appears to have both remote and local sources in that there are time periods when the variance increases in frequency with time (as with swell, i.e., 8/20) and time periods of immediate broadband increases (i.e., 9/02).

As well, two forms of highly intermittent signals appear in the 0.1–10 mHz range of the spectrogram. These are noted in Fig. 5d by black triangles and black circles and are discussed in turn:

- The black triangles at the bottom of Fig. 5d indicate signals that are typically coherent but with varying phase between all three measurement locations (Fig. 1). The signal duration is several hours and is dominated by a few cycles of pressure fluctuations equivalent to several centimeter surface displacement at ≃1-h period. These are likely signatures of mesoscale variability—this will be assessed in a separate investigation from further analysis of the larger moored dataset.
- Finally, groups of nonlinear internal waves appear in the 1–10-mHz range at SW37 and SW38 between 16 August and 26 August. None were observed at SW39 in the measured pressure record. Waves arrived as a packet, first at SW38 and then several hours later as a modified group at SW37. Some named waves tracked by ship did not appear in the pressure record, and many waves that appeared in the pressure record were not tracked by ship. The named waves Rosey, Tonya, and Wyatt correspond to bursts of large spectral amplitudes in the 1–10-mHz range. Other waves such as Sonny and Veda have weaker or more obscured seafloor pressure signals. Prior to Rosey, nonlinear internal wave pressure signals were considerably weaker. In the following analysis, we relate these pressure signals to lander-based velocity profile observations, from which we infer the pressure following Moum and Smyth (2006).

b. Pressure signatures of nonlinear internal waves

The nature of the seafloor pressure signal due to the passage of a nonlinear internal wave is seen by bandpass filtering the measured pressure. Figure 6c shows the result of a low-pass filter at 1/20 Hz and high-pass

[1] Neither tropical storm passed particularly close to the SW06 site, although the effect on both winds and waves was significant. Tropical Storm Ernesto lost strength after crossing the Caribbean islands and then passed over Florida. Tropical Storm Florence passed more than 700 km to the east.

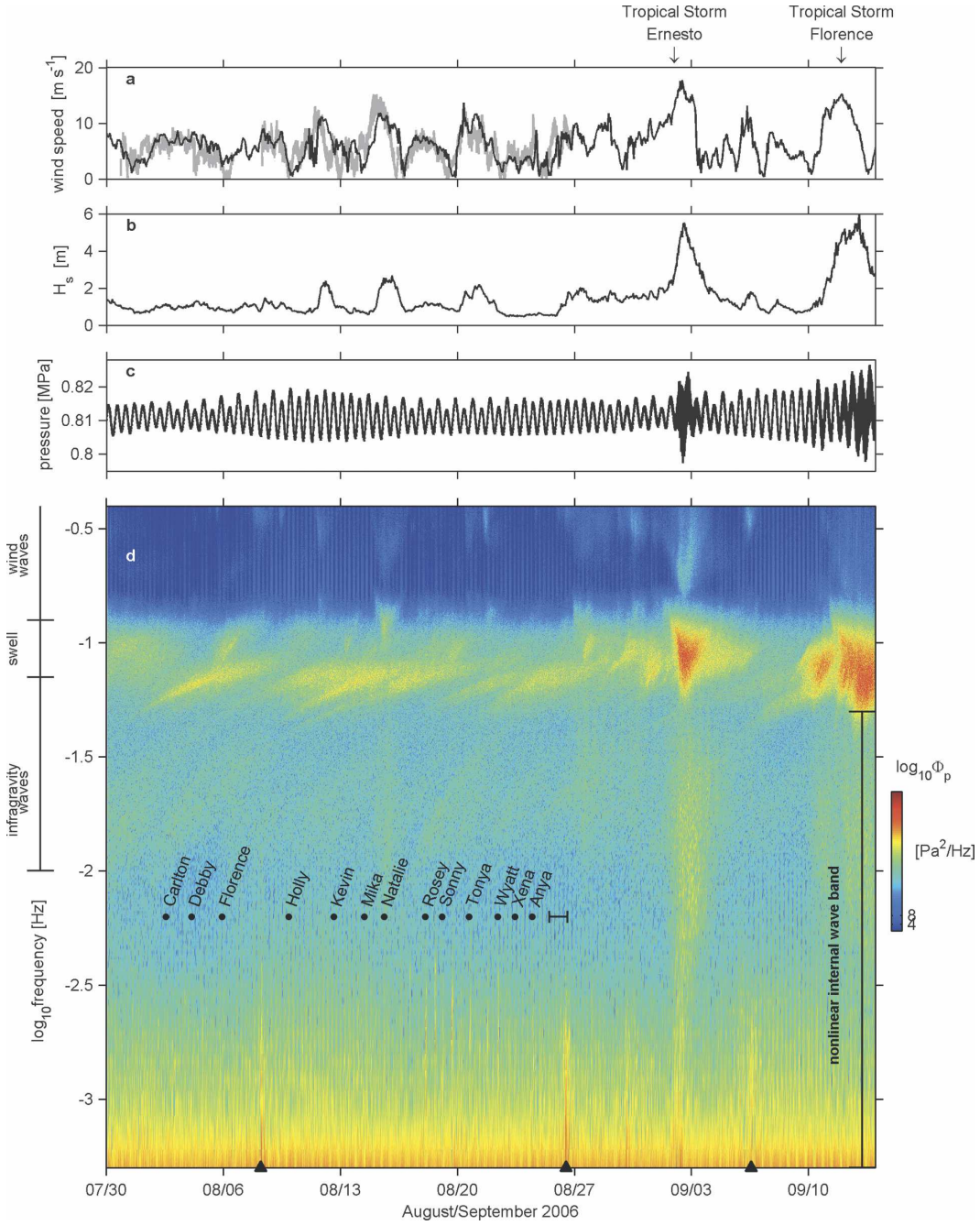

FIG. 5. (a) Wind speeds measured at R/V *Oceanus* during our shipboard experiment (gray) and at NOAA Buoy 44004, 350 km ESE of SW39 (black). (b) Significant wave height (H_s) at NOAA Buoy 44004. (c) Pressure record at SW37, 29 Jul–14 Sep 2006. (d) Spectrogram of the pressure record shown in (c). Individual spectra were computed over 4096 s; hence the tide was not resolved. This record includes the effects of two named tropical storms that are not included in the spectra shown in Fig. 3. Named nonlinear internal wave trains tracked with shipborne measurements through the array are noted at their projected arrival times at SW37. The horizontal line refers to a 26-h profiling time series at SW37, which is referred to in the text. Triangles at bottom denote events noted in text. To the left of (d) are indicated the approximate frequency bands of wind waves, swell, and infragravity waves; at right is shown the nonlinear internal wave band.

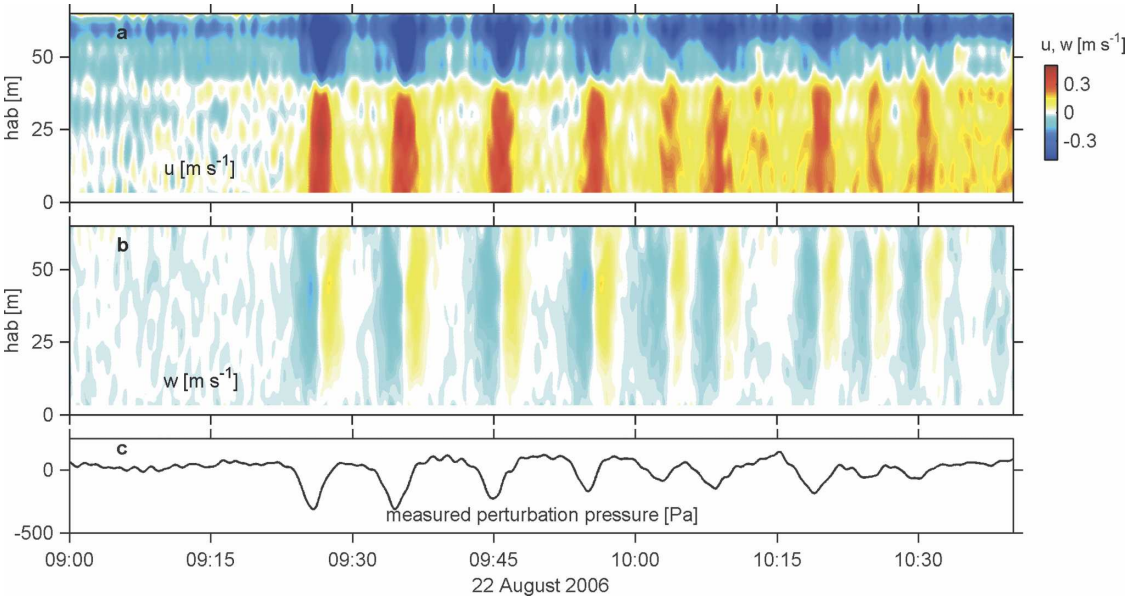

FIG. 6. Time series at SW37 during the passage of wave Wyatt: (a) horizontal velocity in compass direction 120°, (b) vertical velocity, and (c) wave perturbation pressure.

filter at 1/2000 Hz during the passage of wave Wyatt.[2] A sequence of negative pressure perturbations (maximum—350 Pa) corresponds to the distinctive horizontal (Fig. 6a) and vertical (Fig. 6b) velocity signatures of nonlinear internal waves (Moum and Smyth 2006). The waves appear at SW37 at about 0924 UTC 22 August, having passed SW38 almost 4 h earlier (Fig. 7). The wave speed determined from the travel time between SW38 to SW37 is 0.8 m s^{-1}. We have used this particular wave as an example in part because it propagates along a straight line intersecting SW37 and SW38 and in part because its seafloor pressure signal is so clear. Not all large waves have such an unambiguous seafloor pressure signal. During the period shown in Fig. 7, we tracked this wave from ship. X-band radar measurements indicate that wave fronts were aligned (within 5°) perpendicular to the line of intersection of SW37 and SW38. Multiple crossings of the wave front led to an independent estimate of wave speed = 0.8 ± 0.05 m s^{-1}.

A longer time series (Fig. 8) reveals several features. Here, the nonlinear internal wave packets are easily identified by their vertical velocity structure (Fig. 8b) and perturbation pressures (this is simply pressure bandpass filtered at [1/20, 1/2000] Hz; Fig. 8d). The barotropic tide dominates the unfiltered pressure record (Fig. 8c). In this longer record

- we observed nonlinear internal wave groups with significantly larger negative pressure perturbations than Wyatt. Rosey exhibited the largest signal.
- not all wave packets have a strong near-bottom velocity and, therefore, pressure signal. Sonny, Veda, and the wave preceding Tonya are examples.
- wave groups consistently appear with the surface-intensified shoreward velocity that is presumably part of the internal tide.
- while nonlinear internal waves do appear close to semidiurnal during this period, they are not phase-locked to the barotropic tide, but instead wander in phase by several hours.
- during this time period, these waves appear exclusively during the low to rising surface tide at this site and, thus, are examples of the tendency in timing suggested by Fig. 2.

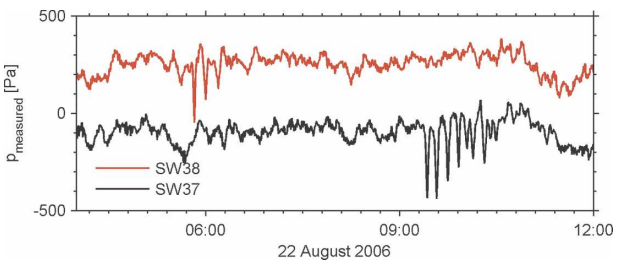

FIG. 7. Time series of wave pressure at SW37 and SW38 during the passage of wave Wyatt. The signals have been offset in amplitude for clarity.

[2] We later employ Wyatt as a pedagogical example in comparing measured and inferred wave pressure signals.

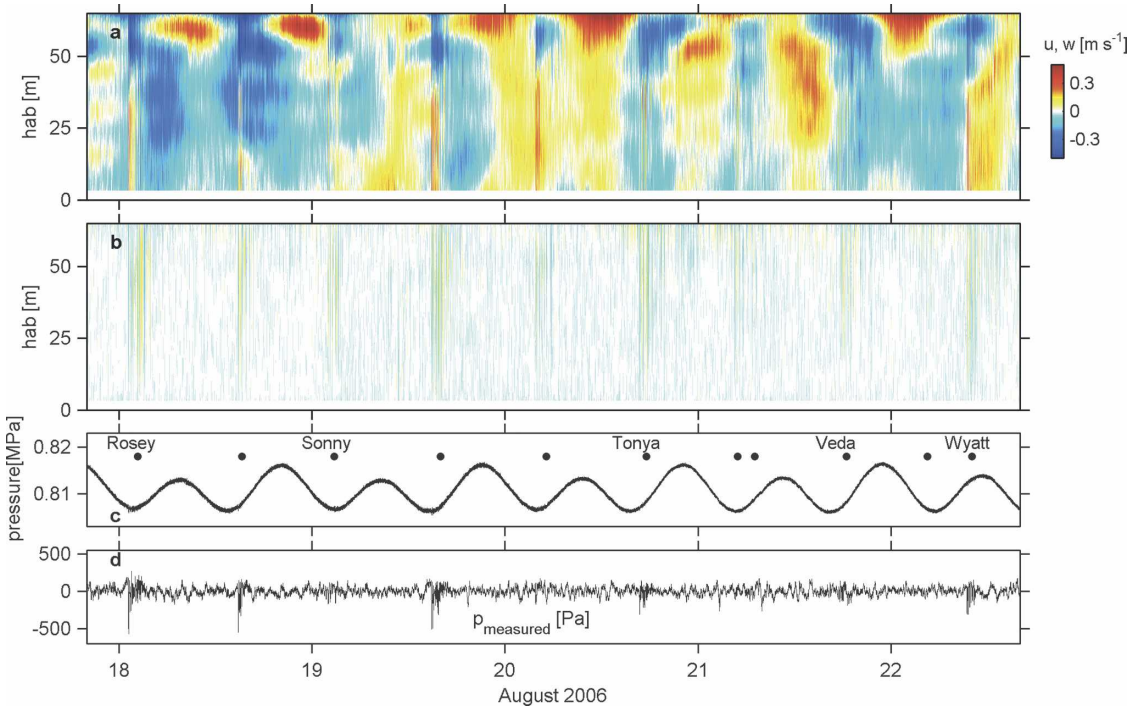

FIG. 8. Five-day time series at SW37 of (a) horizontal velocity in compass direction 120°; (b) vertical velocity; (c) seafloor pressure; (d) seafloor pressure low passed at 1/20 s and high passed at 1/2000 s. Note that 1 Pa is equivalent to 1 N m^{-2}. Named nonlinear internal wave trains tracked from R/V *Oceanus* during this period are noted in (c). Additional waves (unnamed) detected from the vertical velocity record and noted in Fig. 2 are also shown.

c. *Comparison of inferred and measured wave pressure*

In this section, the pressure signal due solely to the internal wave is inferred first from the horizontal momentum equation as (7) and compared to the measured seafloor pressure. Then the component pressures are determined from the vertical momentum equation through (2), summed, and similarly compared.

ADP measurements from the lander begin at 3.2-m height above the seafloor. Any systematic differences between the velocity at this height and $z = 0+$ will lead to inaccuracy in the seafloor pressure inferred from (7). Assuming the wave propagates without change of form, $dx = cdt$, where the wave speed c in this example (wave Wyatt) is determined to be 0.8 m s^{-1} independently from differencing arrival times at SW37/SW38 and from shipboard wave-tracking measurements. The integration was started 15 min prior to the arrival of the leading wave and continued through the passage of the third wave in the group (Fig. 9). This is compared to the bandpassed ([1/20, 1/2000] Hz) pressure record. While the amplitude of $p^0_{Du/Dt}$ is somewhat smaller than the measured pressure, the sign, timing, and trend of the inferred signal is correct.

To infer pressure from (2), we require complete density and velocity fields through the wave. First, we applied the modified beam-to-earth transformation described by Scotti et al. (2005) to ADP velocity profiles in order to minimize beam-spreading attenuation of sharp features at long range from the transducer. Then, following Moum and Smyth (2006), we used these velocity fields to reconstruct the density field of the wave. With the assumption that the waves are inviscid, two-dimensional and propagate without change in shape with known speed and direction, isopycnals parallel streamlines. Using a background density profile obtained from shipboard profiling, isopycnals were mapped to streamlines computed from the velocity

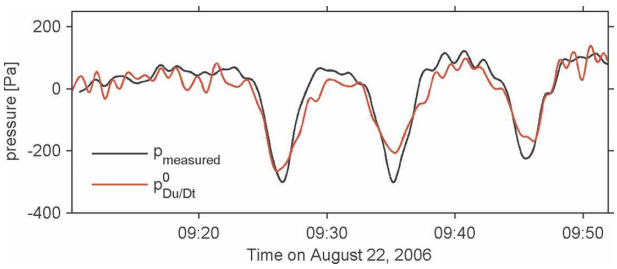

FIG. 9. Measured wave perturbation pressure (black) and wave pressure estimated from horizontal momentum equation using the velocity measured at 3.2 m above the seafloor [red; Eq. (7)].

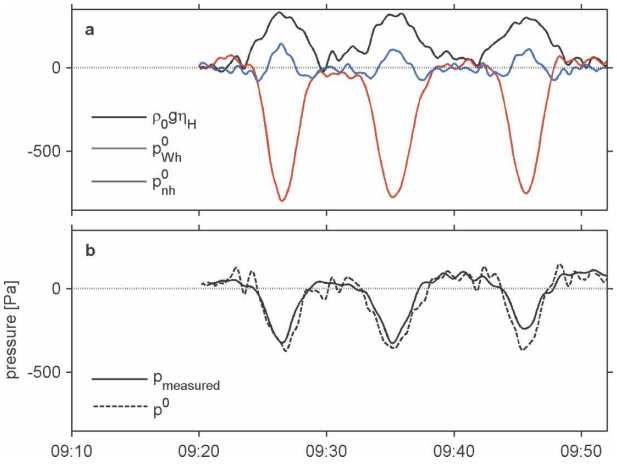

FIG. 10. (a) Estimated external hydrostatic pressure $\rho_0 g\eta_H$, internal hydrostatic pressure p^0_{Wh}, and nonhydrostatic pressure (p^0_{nh}), evaluated at the seafloor through wave Wyatt. (b) Total estimated seafloor pressure p^0 and measured seafloor pressure.

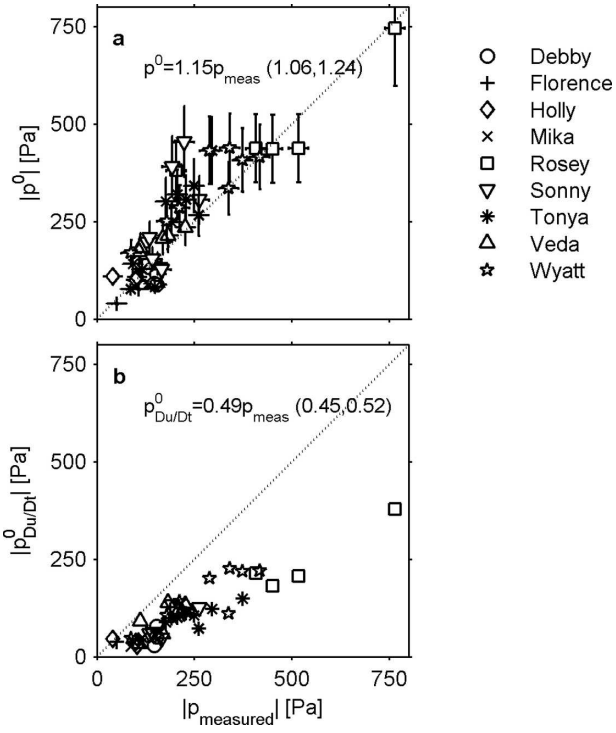

FIG. 11. Plot of (a) $|p_{\mathrm{measured}}|$ vs $|p^0|$ for the leading three–eight waves in each of the measured wave packets identified in the legend. Confidence limits represent upper bounds; ±20% of $|p^0|$ and ±25 Pa for the measured pressure. (b) As in (a) but for $|p_{\mathrm{measured}}|$ vs $|p^0_{Du/Dt}|$. Neutral regression fits with 95% confidence intervals are shown.

measurements. The resulting pressure components, evaluated at the seafloor, are shown in Fig. 10a. The total seafloor pressure inferred from (2) is compared to the measured pressure perturbation in Fig. 10b. The general correspondence between inferred and measured pressure is quite good, although the inferred pressure appears to be slightly larger.

6. Discussion

Moum and Smyth (2006) found that inferred wave pressure maxima, $|p^0|$, were consistently greater than $|p^0_{Du/Dt}|$.The pressure measurements here indicate that $|p^0_{Du/Dt}| < |p_{\mathrm{measured}}| < |p^0|$ (in this case, $|\cdots|$ refers to wave pressure minima). This is seen in our example waves (Figs. 9, 10) and is a consistent result that ensues from an analysis of the leading three–eight waves of each of the named wave packets identified in Fig. 11.[3]

It is possible that $|p^0|$ is an overestimate simply due to inadequate velocity measurement near the sea surface. Although we have tried to correct for beam attenuation at long range, this correction is imperfect to some unknown extent. We also have no velocity measurements in the upper 12 m, where we expect the velocities in a depression wave to be most intense, so we have extrapolated from an imperfect measurement at 12 m. As a consequence, we have certainly underestimated the magnitude of Du/Dt at $z = H$ and, therefore, $\rho_0 g\eta_H$. Since the external hydrostatic pressure is of opposite sign to the dominant internal hydrostatic pressure, and p^0, this leads to an overestimate of the magnitude of p^0. Because of the same measurement limitations, it is also likely that vertical accelerations are underestimated near the surface, and (p^0_{nh}), is underestimated, again contributing to an overestimate of the magnitude of p^0.

As discussed by Moum and Smyth (2006), since $u = 0$ at the seafloor, the balance of horizontal momentum there differs from (7); at $z = 0$ the horizontal pressure gradient balances the vertical divergence of the turbulence stress. The change in sign of $\partial p/\partial x$ across the wave provides some insight into the structure of the turbulence above the seafloor. We have assumed a perfect balance between $\partial p/\partial x$ and $\rho_0 Du/Dt$ at $z = 3.2$ m, and therefore a sharp change in dynamics over a limited depth range. It is possible that our assumption is incorrect because of an unknown contribution from the turbulence stress divergence at $z = 3.2$ m. In fact, since the turbulence stress divergence must have the same sign as $\partial p/\partial x$ at $z = 0$, we suspect it may also some small but finite distance from the seafloor as well, and thus tend

[3] The waves selected for this analysis had known wave speed and direction from wave-tracking experiments, and pressure minima could be unambiguously determined from measurements, (2) and (7). It was frequently the case that trailing waves were less distinct.

to reduce the magnitude of $p^0_{Du/Dt}$ relative to the measured pressure. It is also possible that there is a real diminution of the magnitude of the wave pressure at 3.2-m height, below its seafloor value.

The analysis summarized by Fig. 11 also indicates the range of measured pressures. The maximum observed pressure signal in these waves of depression was 765 Pa, roughly three times that induced by the largest waves of elevation observed by Moum and Smyth (2006) over the Oregon continental shelf. For the seafloor pressure measurements, our estimated uncertainties are reasonably small as shown in Fig. 11a. The primary source of error is associated with the filtering necessary to extract the nonlinear internal wave signal from the total pressure measurement. The nonlinear internal wave signal is small relative to the tide (Fig. 5c) and comparable to that of swell in 70-m water depth. Fortunately, nonlinear internal waves occupy a frequency band unique from these two regular signals. This helps to define the filter cutoff frequencies used to extract the nonlinear internal wave pressure signal. However, the filter cutoff frequencies are not unambiguous and other, less regular, phenomena contribute to the pressure signal. By changing filter cutoff frequencies over a reasonable range that also removes swell and tide, we have conservatively estimated the uncertainty in a particular estimate derived from the filtered pressure measurement to be ± 25 Pa. Instrument noise associated with the Paroscientific sensor (<2 Pa rms) is negligible. Uncertainties associated with inferring pressure from ADCP velocities were estimated by Moum and Smyth (2006) to be $\pm 20\%$ for waves of elevation on the Oregon coast. We assume the same fractional uncertainty to determine the error in $|p^0|$ for the waves of depression presented here; we have not explicitly accounted for error associated with our inadequate velocity measurements near the sea surface.

The waves detected in our seafloor pressure measurements evolved considerably over the 11-km propagation range between SW38 and SW37 (one example is shown in Fig. 7).[4] This evolution includes changes in wave amplitude, spacing between waves, and number of waves in a wave packet. Despite the changes between observation sites, we are confident in our identification of *named* waves in the pressure records since their history is known from shipboard measurements through the moored array and wave speeds are consistent between that portion of the array.

The structural evolution between SW37 and SW38 should not negate our assumption that the waves propagate without change of form over a single wavelength. In a separate analysis of energy losses from nonlinear internal waves of similar speed and amplitude as those described herein, and propagating over the Oregon shelf (Moum et al. 2007a), we found that half of their energy was lost in 12 h. If this rate of energy change was constant (which it is not), it would correspond to less than 1% change over a 10-min wave period. These calculations have yet to be done for the waves observed over the New Jersey shelf, but, as the New Jersey shelf has shallower slope, we expect the Oregon example to be an upper bound to our estimate. In addition, it is reasonable to consider the result summarized by Figs. 10b and 11a to support our constancy-of-form assumption.

The timing of the waves is not fixed relative to the barotropic tide (Figs. 2, 8). This was also the case for nonlinear waves of elevation observed over the Oregon continental shelf (Moum et al. 2007b). However, we suspect the energy source of the nonlinear internal waves to be the tides and that variations in arrival times at a location remote from the generation site may be due to several factors: changes in the wave generation location (yet to be identified) due to mesoscale modulation of stratification; changes in wave propagation speed due to varying stratification and/or larger-scale currents along its path; and changes in wave direction due to interaction with other waves, a phenomenon observed several times from shipboard wave-tracking experiments. Further analysis employing the full suite of experiment measurements is focused on defining the wave generation mechanisms, with the intent of explaining both the unanticipated spring/neap correspondence and the variations in arrival times at a location on the shelf.

Many of the waves that were tracked, or were detected from the vertical velocity record (as in Fig. 2), have weak or no seafloor pressure signal (Fig. 8). This means that the sum of the internal plus external hydrostatic pressures plus nonhydrostatic pressure is small or zero at the seafloor. More directly, it means that Du/Dt is small or zero at the seafloor. A rudimentary nonlinear internal wave detector utilizes the rectified pressure signal, bandpassed over the frequency band (1/1000, 1/100) Hz (Fig. 12).[5] Many more waves were defined from the vertical velocity 40 m above the seafloor than are clearly evident in the rectified, bandpassed pres-

[4] The 11-km range is equivalent to ~50 wavelengths of a 200-m wavelength wave, or 4-h travel time at $c = 0.8\ \mathrm{m\ s^{-1}}$.

[5] We found empirically that the bandwidth (1/1000, 1/100) Hz was a better rms discriminator of nonlinear internal waves than what we have used to compute $|p_{\mathrm{measured}}|$ and to present the time series in previous figures.

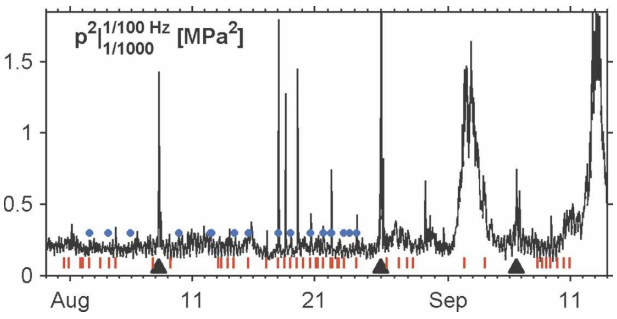

FIG. 12. Squared pressure, bandpassed at (1/1000, 1/100) Hz. The blue dots represent arrival times of named nonlinear internal waves determined from ship-tracking experiments. The red ticks represent nonlinear internal waves identified from the vertical velocity profile record at SW37 and plotted in Fig. 2. Triangles are the disturbances noted in Fig. 5d.

sure. While the most intense waves are detected, many are not, simply because the wave velocities in depression waves are most intense near the sea surface. In deep water, the seafloor pressure signal of a wave of depression must vanish. On the other hand, because their wave velocities are most intense immediately above the seafloor, elevation waves will have more consistent seafloor pressure signals, independent of H.

7. Summary and conclusions

The purpose of these seafloor pressure measurements was to confirm the nonlinear internal wave pressure inferred by Moum and Smyth (2006). We believe that the measurements provide adequate experimental verification. In turn, we can assume that we now have a detailed understanding of the pressure field in the waves. Most importantly, since the pressure–velocity correlation represents an important component of the wave energy flux, it also means that we understand the components of, and the spatial distribution of, energy transport in the waves as well as the *net* energy transport by the waves (Moum et al. 2007b).

The arrivals of nonlinear internal waves were not phase-locked to the tide, a factor that should not discount the tide as an energy source for their generation. They do appear to be generally in phase with a velocity signal that we assume to be part of the internal tide and they occur predominantly during low and rising tides.

While a seafloor pressure measurement is an inconsistent means of detecting surface-trapped nonlinear internal waves of depression (at least those of smaller amplitude), and is useless for this purpose in deep water, it represents a reliable detector of bottom-trapped nonlinear internal waves of elevation.

Acknowledgments. This work was funded by the Office of Naval Research. We are grateful to Ray Kreth and Mike Neeley-Brown for their technical expertise, to them and Emily Shroyer, Sam Kelly, and Greg Avicola for help in obtaining the data, to Alexander Perlin for help in organizing data, and to the captain and crew of the R/V *Connecticut* and to Jim Ryder (WHOI) for their help in recovering our bottom landers under trying circumstances. The captain and crew of the R/V *Oceanus* were most helpful in support of our wave-tracking experiment. The constructive comments of Bill Smyth, Parker MacCready, and two anonymous reviewers are appreciated.

REFERENCES

Helfrich, K. R., and W. K. Melville, 2006: Long nonlinear internal waves. *Annu. Rev. Fluid Mech.,* **38,** 395–425.

Kunze, E., L. K. Rosenfeld, G. S. Carter, and M. C. Gregg, 2002: Internal waves in Monterey Submarine Canyon. *J. Phys. Oceanogr.,* **32,** 1890–1913.

Meinig, C., S. E. Stalin, A. I. Nakamura, F. Gonzalez, and H. B. Milburn, 2005: Technology developments in real-time tsunami measuring, monitoring and forecasting. *Oceans 2005, MTS (Marine Technology Society)/IEEE Proceedings,* Vol. 2, IEEE, 1673–1679.

Moum, J. N., and W. D. Smyth, 2006: The pressure disturbance of a nonlinear internal wave train. *J. Fluid Mech.,* **558,** 153–177.

——, M. C. Gregg, R. C. Lien, and M. E. Carr, 1995: Comparison of turbulence kinetic energy dissipation rate estimates from two ocean microstructure profilers. *J. Atmos. Oceanic Technol.,* **12,** 346–366.

——, D. M. Farmer, E. L. Shroyer, W. D. Smyth, and L. Armi, 2007a: Dissipative losses in nonlinear internal waves propagating across the continental shelf. *J. Phys. Oceanogr.,* **37,** 1989–1995.

——, J. M. Klymak, J. D. Nash, A. Perlin, and W. D. Smyth, 2007b: Energy transport by nonlinear internal waves. *J. Phys. Oceanogr.,* **37,** 1968–1988.

Nash, J. D., M. H. Alford, and E. Kunze, 2005: Estimating internal wave energy fluxes in the ocean. *J. Atmos. Oceanic Technol.,* **22,** 1551–1570.

Scotti, A., B. Butman, R. C. Beardsley, P. S. Alexander, and S. Anderson, 2005: A modified beam-to-earth transformation to measure short-wavelength internal waves with an acoustic Doppler current profiler. *J. Atmos. Oceanic Technol.,* **22,** 583–591.

Webb, S. C., X. Zhang, and W. Crawford, 1991: Infragravity waves in the deep ocean. *J. Geophys. Res.,* **96,** 2723–2736.

CORRIGENDUM

There was a press error in Fig. 10 of Moum and Nash (2008). The legend in Fig. 10a was shown in black and white instead of color. The correct figure and caption as they were meant to appear are shown below.

The staff of the *Journal of Physical Oceanography* regrets any inconvenience this error may have caused.

REFERENCE

Moum, J. N., and J. D. Nash, 2008: Seafloor pressure measurements of nonlinear internal waves. *J. Phys. Oceanogr.,* **38,** 481–491.

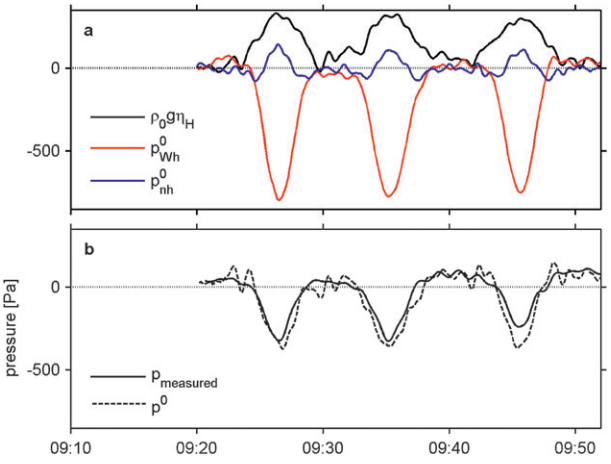

FIG. 10. (a) Estimated external hydrostatic pressure $\rho_0 g\eta_H$, internal hydrostatic pressure p^0_{Wh}, and nonhydrostatic pressure (p^0_{nh}), evaluated at the seafloor through wave Wyatt. (b) Total estimated seafloor pressure p^0 and measured seafloor pressure.

DOI: 10.1175/2010JPO4444.1